Supporting Information

Flexible, High Power Density, Wearable Thermoelectric Nanogenerator and Self-powered Temperature Sensor

Rui Feng [a,b], *Fei Tang* [a,b,*], *Ning Zhang* [c], *Xiaohao Wang* [a,b]

[a] Department of Precision Instrument, Tsinghua University, Beijing, 100084, China

[b] State Key Laboratory of Precision Measurement Technology and Instruments, Tsinghua University, Beijing, 100084, China

[c] Quantum Sensing Center, Zhejiang Lab, Hangzhou, 310000, China

Corresponding Author

Auth: Fei Tang

Addr: Department of Precision Instrument, Tsinghua University, Beijing, 100084, China

Email: tangf@mail.tsinghua.edu.cn

Tel: +86 010 62796216

Section 1 Operating Principle of Thermoelectric Energy Harvester

A thermoelectric energy harvester is essentially a thermopile composed of a plurality of N-type and P-type thermoelectric semiconductor materials in a certain arrangement. In order to facilitate modelling analysis, only an idealized thermoelectric nanogenerator (TEG) consisting of a N-type and a P-type thermoelectric semiconductor is considered here, where the N-type and P-type thermocouple legs are connected via three metal conductors (such as copper foil) with negligible resistance (as shown in Figure S1). The TEG operates between cold and heat sources, where the hot side absorbs heat from the heat source T_1 and then the cold side releases heat to the cold source T_2, to convert thermal energy into electric energy, and then output it in the form of thermoelectromotive force or electric power.

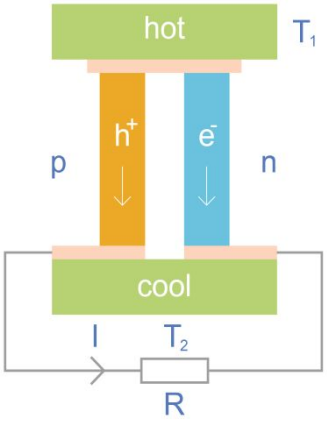

Figure S1. Operating principle of single thermocouple

From the energy-balance equation, it can be found that in the N-type and P-type thermocouple legs, the heat Q_n and Q_p transferred from the heat source to the cold source are:

$$Q_n = -\alpha_n I T - \kappa_n A_n \frac{dT}{dx} \quad (1)$$

$$Q_p = \alpha_p I T - \kappa_p A_p \frac{dT}{dx} \quad (2)$$

where α refers to the absolute Seebeck coefficient of materials; I refers to the output current; κ refers to the thermal conductivity of materials; A refers to the cross-sectional area of the thermocouple leg; dT/dx refers to the temperature gradient in the thermocouple leg.

If the Thomson effect of the current is ignored, the relationship between the temperature

gradient in the N-type and P-type thermocouple legs and the Joule heat per unit length is as follows:

$$-\kappa_{\mathrm{n}} A_n \frac{d^2T}{dx^2} = \frac{I^2}{A_{\mathrm{n}}\sigma_n} \tag{3}$$

$$-\kappa_{\mathrm{p}} A_p \frac{d^2T}{dx^2} = \frac{I^2}{A_{\mathrm{p}}\sigma_p} \tag{4}$$

The boundary conditions are set as follows:

At the hot side, when x=0, $T = T_1$;

At the cold side, when $x = L_n$ or $x = L_p$, $T = T_2$.

Here, σ refers to the electrical conductivity of materials; L_n refers to the length of the N-type thermocouple leg; and L_p refers to the length of the P-type thermocouple leg.

To substitute boundary conditions into Equations (3) and (4) and then solving them, the following results can be obtained:

$$\kappa_{\mathrm{n}} A_n \frac{dT}{dx} = \frac{I\left(x - L_n/2\right)}{\sigma_n A_n} + \frac{\kappa_n A_n \left(T_2 - T_1\right)}{L_n} \tag{5}$$

$$\kappa_{\mathrm{p}} A_p \frac{dT}{dx} = \frac{I\left(x - L_p/2\right)}{\sigma_p A_p} + \frac{\kappa_p A_p \left(T_2 - T_1\right)}{L_p} \tag{6}$$

By substituting Equations (5) and (6) into Equations (1) and (2) respectively and then solving them, the heat absorption Q1 and heat release Q2 of the TEG power generation cycle can be obtained as follows:

$$\mathrm{Q}_1 = \left(\alpha_{\mathrm{p}} - \alpha_n\right) I T_1 + K\left(T_1 - T_2\right) - I^2 R/2 \tag{7}$$

$$\mathrm{Q}_2 = \left(\alpha_{\mathrm{p}} - \alpha_n\right) I T_2 + K\left(T_1 - T_2\right) - I^2 R/2 \tag{8}$$

where:

$$K = \frac{\kappa_n A_n}{L_n} + \frac{\kappa_p A_p}{L_p}$$

$$R = \frac{L_n}{\sigma_n A_n} + \frac{L_p}{\sigma_p A_p}$$

$$\alpha = \alpha_p - \alpha_n$$

K refers to the total thermal conductivity of the thermocouple leg; R refers to the total electrical conductivity of the thermocouple leg; α refers to the total Seebeck coefficient of the thermocouple leg.

The power P and efficiency η of the TEG power generation cycle are as follows:

$$P = Q_1 - Q_2 = I(T_1 - T_2)\alpha - I^2 R \tag{9}$$

$$\eta = \frac{P}{Q_1} \times 100\% \tag{10}$$

This is because the dimensionless figure of merit ZT of thermoelectric materials is defined as:

$$ZT = \frac{\alpha^2 RT}{K} \tag{11}$$

where T refers to the absolute temperature.

Combining (9) and (11), it can be found that at the maximum power output (∂P/ ∂I = 0), the cycle efficiency is as follows:

$$\eta = 2ZT\left(1 - \frac{T_2}{T_1}\right) \Big/ \left[ZT\left(3 + \frac{T_2}{T_1}\right) + 8\right] \tag{12}$$

As can be seen from the above equation, the larger the dimensionless figure of merit ZT of the material is, the higher the power generation efficiency of the TEG is. Therefore, the ideal state is that a material features a high α and σ value but a low k value. According to Wiedemann-Franz's law, however, for the ratio of electrical conductivity to thermal

conductivity of a material is constant, it is impossible to increase the electrical conductivity of a material and reduce its thermal conductivity at the same time. Furthermore, it is found that the property of a thermoelectric material is related to not only the material itself, but also the temperature of the environment where the material is located. The thermoelectric properties of materials vary with temperature, and only at a certain temperature or temperature range can thermoelectric materials have the best thermoelectric properties. Figure S2 shows the changes in the thermoelectric figure of merit ZT of various thermoelectric materials as a function of temperature after consulting the relevant literature[1]. In the scene where the thermoelectric energy harvester is used in this study, Bi_2Te_3 is the ideal choice at room temperature.

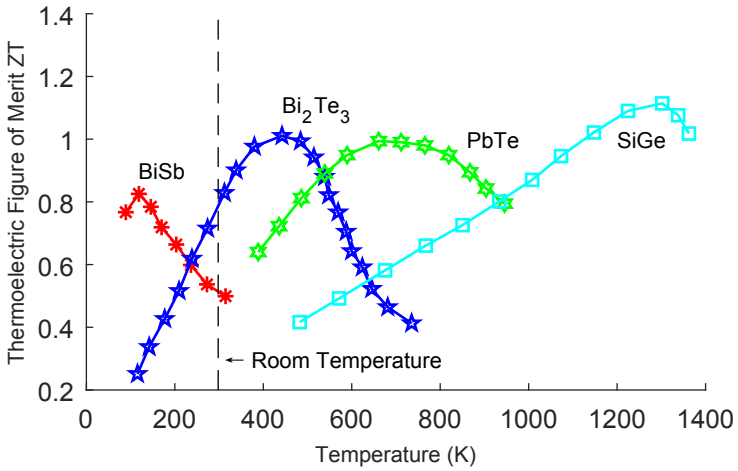

Figure S2. Thermoelectric figure of merit ZT as a function of temperature

Section 2 Process Steps

The process program is shown in Figure S3, and the detailed steps are as follows:

1. Remove the surface oxidant of bismuth block, antimony block, selenium block and tellurium block with a purity of 4N, and then pulverize them by a ball mill;

2. Seal one end of the glass tube (inner diameter of 10~38mm) with a propane or gas lamp and anneal it fully. Melt, smooth and clean the other end with glass cleaner, purified water, acetone and deionized water, and then dehydrate it with alcohol and dry for use;

3. Proportion the samples according to the molar ratio of stoichiometric $(Bi_xSb_{1-x})_2Te_3$ (x=0.24~0.26 P-type thermoelectric materials) and $Bi_2(Te_{1-x}Se_x)_3$ (x=0.02~0.1 N-type thermoelectric materials);

4. Vacuum the glass tube with materials to a pressure below 10Pa and seal it at a distance of 3 to 5 cm from the material plane;

5. Place the sealed glass tube in a rocking furnace at 500~550°C and rock it horizontally by more than ±15^o at a frequency of 1 to 3Hz until all the materials are molten. Keep on rocking for 3 minutes to make the materials mix evenly, and then place it in an exhaust furnace where the liquid material is to be vibrated and vented for 5 minutes, then erect it in the air for natural cooling;

6. Open the cooled P/N type glass tube, place the pre-cut P/N type seed crystal therein, and vacuum and seal it again;

7. Erect the glass tube with seed crystal, put it into a zone-melting furnace for zone-melting, keep the zone-melting temperature at 600~650°C, the zone-melting width at 3~5cm, and the growth rate at 3.0±1.0cm/h, and cool it in the air naturally after the growth is completed;

8. Anneal the zone-melted crystal bar in an annealing furnace at 380±50°C for more than 36 hours, and then cool it with the furnace;

9. Break the outer glass rod, cut off both ends of the crystal bar, and then cut it into slices by wire-electrode cutting;

10. Place the slices into a plating bath, and plate the upper and lower surfaces with tin;

11. After plating, cut them into single thermocouple legs of the desired sizes and shape with laser.

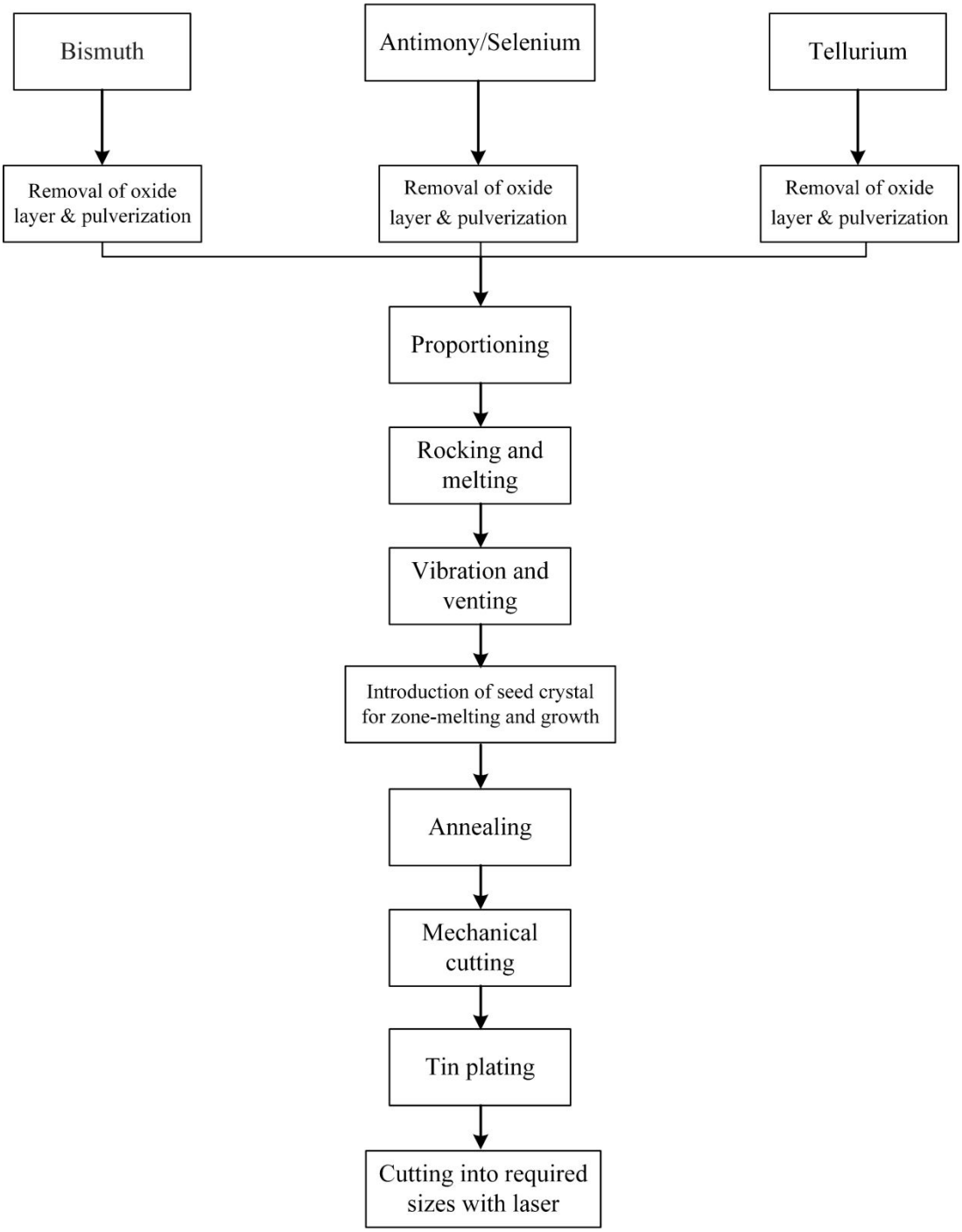

Figure S3. Manufacturing process flow chart

Section 3 Supplementary Figures

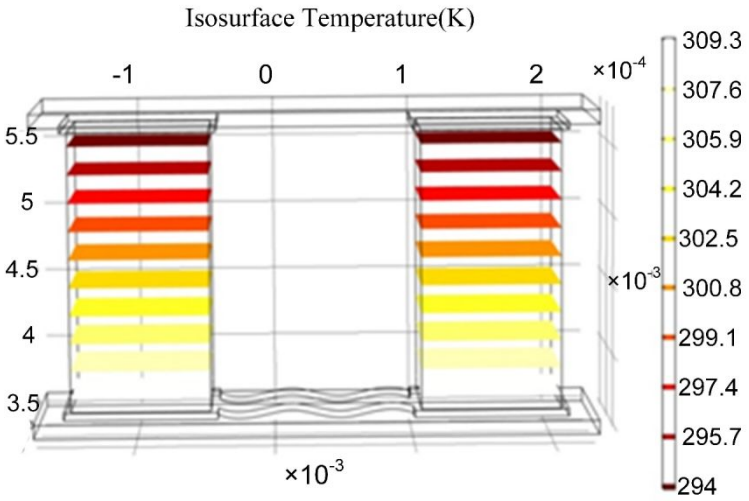

Figure S4. Simulation of the isothermal field distribution across the single TE (T_{cold} = 293K, T_{hot} = 310K)

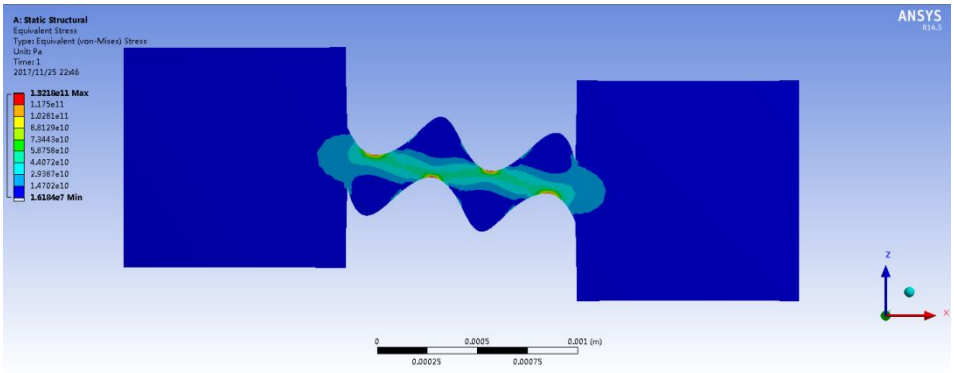

Figure S5. Simulation of the stress distribution during stretching

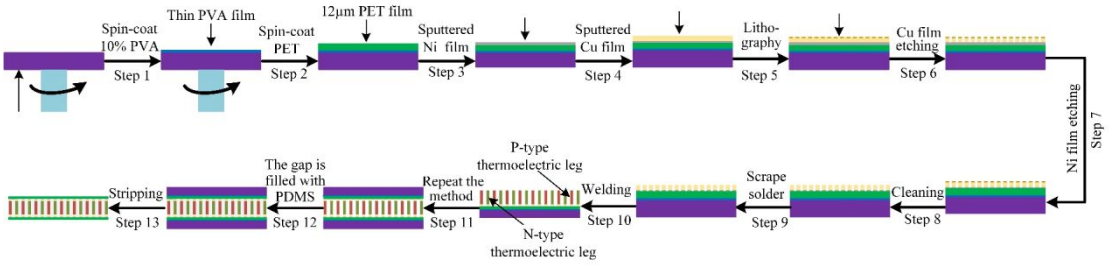

Figure S6. Schematic illustration of the fabrication process of an FTEG

Figure S7. Thickness measurement

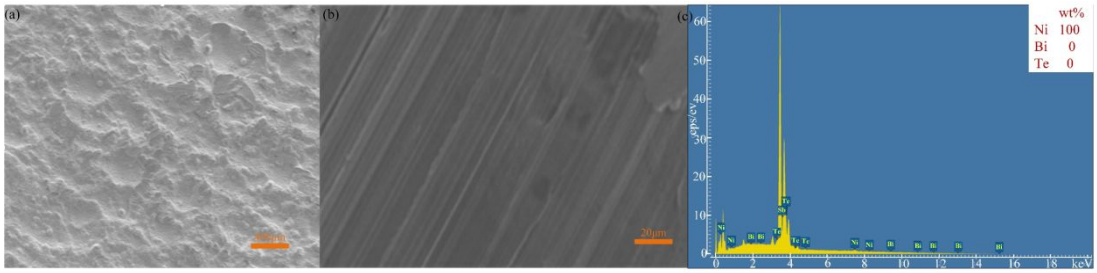

Figure S8. (a) SEM image of surface view of the nickel-plated thermoelectric material. (b) High magnification SEM image of surface view of the nickel-plated thermoelectric materials. (c) EDS spectrum of nickel- plated thermoelectric materials, respectively.

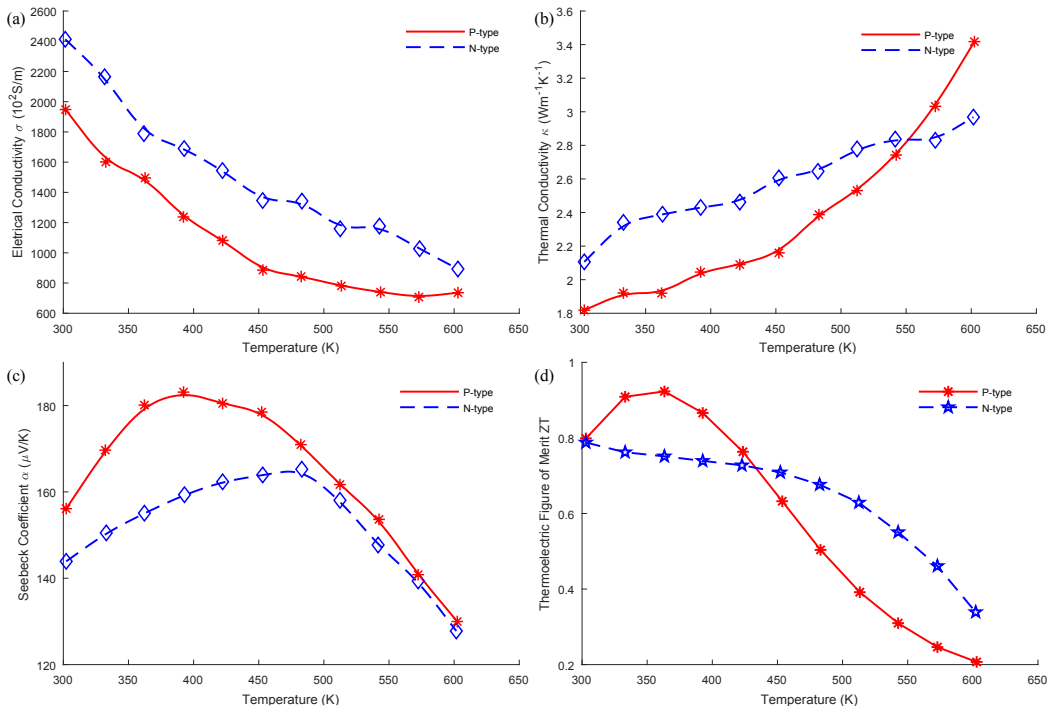

Figure S9. Thermoelectric characteristics of nickel-plated thermoelectric materials after one month of operation: (a) Electrical conductivity. (b) Thermal conductivity. (c) Seebeck coefficient. (d) Thermoelectric figure of merit ZT

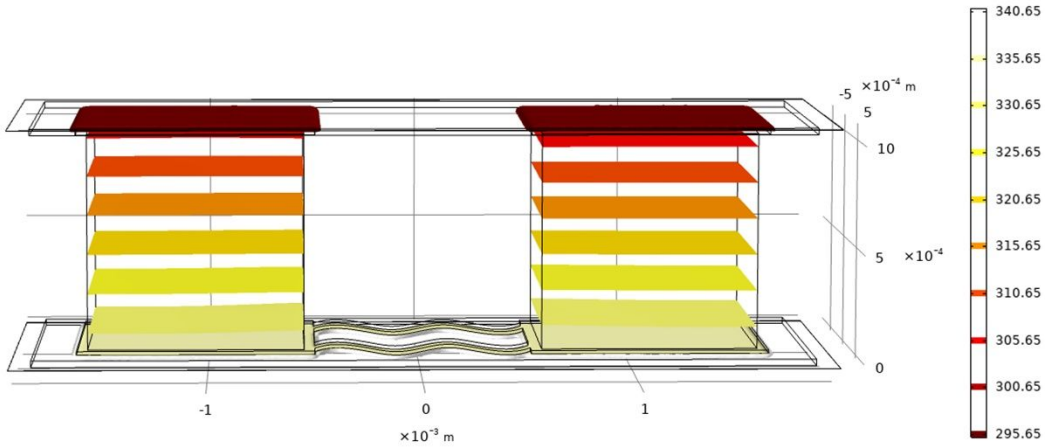

Figure S10. Simulation of the isothermal field distribution across the single TE (T_{cold} = 293K, T_{hot} = 343K)

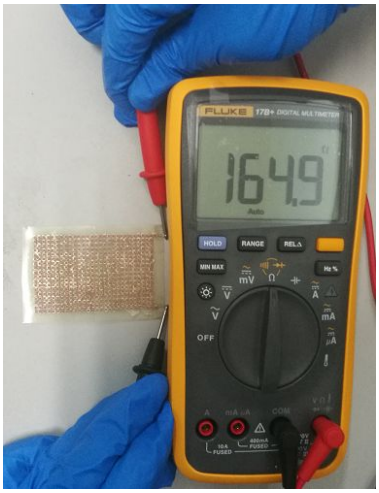

Figure S11. Resistance measurement

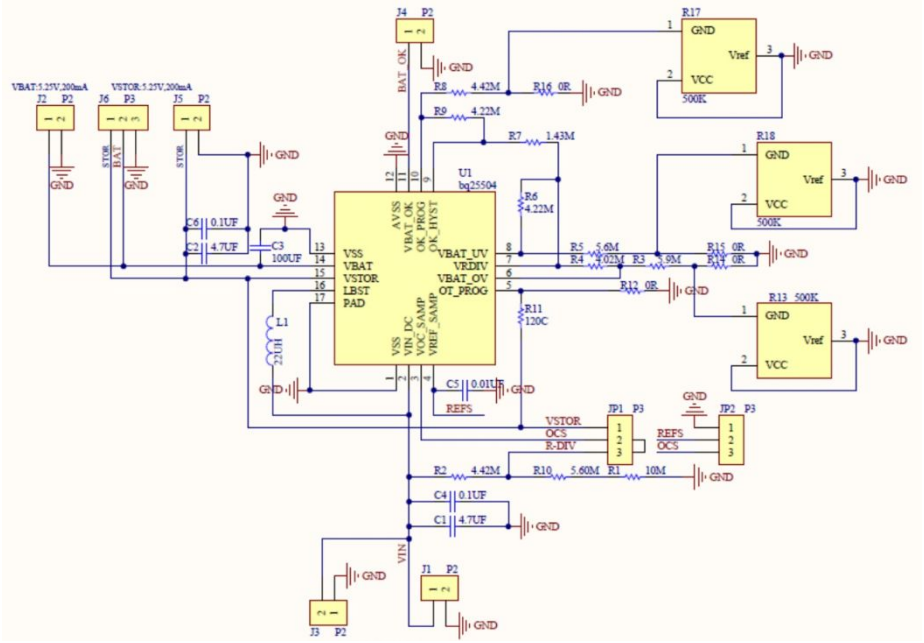

Figure S12. Schematic of boost circuit

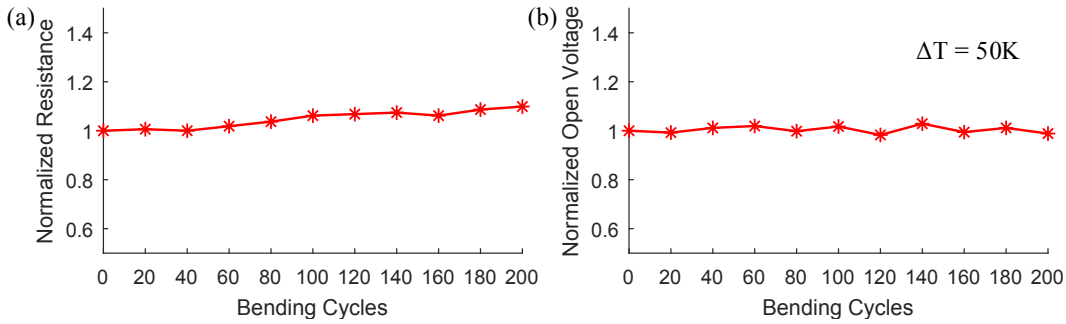

Figure S13. Reliability test by repeated bending cycles: (a). Internal resistance stability. (b). The output open voltage.

Table S1. Comparison of previously reported thermoelectric nanogenerator with the present work

Material	Temperature Difference	Power Density	Refs.
Bi_2Te_3/ Sb_2Te_3	50K	3.8 mW·cm^{-2}	2
pSi	31.5K	12.3 μW·cm^{-2}	3
P_3HT	55K	1.22 μW·cm^{-2}	4
Bi_2Te_3/ Sb_2Te_3	52.5K	9.2 mW·cm^{-2}	5
Bi_2Te_3/Sb_xTe_y	50K	5.3 mW·cm^{-2}	6
$(Bi, Sb)_2Te_3$	20K	40 μW·cm^{-2}	7
Bi_2Te_3/ Sb_2Te_3	22.3K	5.9 μW·cm^{-2}	8
Bi_2Te_3 doped with Sb and Se	50K	11.14 mW·cm^{-2}	This paper

Supplementary References

1. Snyder, G. J.; Toberer, E. S., Complex thermoelectric materials. *Nat. Mater.* **2008,** *7* (2), 105-114.
2. Kim, S. J.; We, J. H.; Cho, B. J., A wearable thermoelectric generator fabricated on a glass fabric. *Energy Environ. Sci.* **2014,** *7* (6), 1959-1965.
3. Ziouche, K.; Yuan, Z.; Lejeune, P.; Lasri, T.; Leclercq, D.; Bougrioua, Z., Silicon-Based Monolithic Planar Micro Thermoelectric Generator Using Bonding Technology. *J. Microelectromech. Syst.* **2017,** *26* (1), 45-47.
4. Yang, Y.; Lin, Z. H.; Hou, T.; Zhang, F.; Wang, Z. L., Nanowire-composite based flexible thermoelectric nanogenerators and self-powered temperature sensors. *Nano Res.* **2012,** *5* (12), 888-895.
5. Zhang, W. H.; Yang, J. K.; Xu, D. Y., A High Power Density Micro-Thermoelectric Generator Fabricated by an Integrated Bottom-Up Approach. *J. Microelectromech. Syst.* **2016,** *25* (4), 744-749.
6. Roth, R.; Rostek, R.; Cobry, K.; Kohler, C.; Groh, M.; Woias, P., Design and Characterization of Micro Thermoelectric Cross-Plane Generators With Electroplated Bi2Te3, SbxTey, and Reflow Soldering. *J. Microelectromech. Syst.* **2014,** *23* (4), 961-971.
7. Snyder, G. J.; Lim, J. R.; Huang, C. K.; Fleurial, J. P., Thermoelectric microdevice fabricated by a MEMS-like electrochemical process. *Nat. Mater.* **2003,** *2* (8), 528-531.
8. Kim, M. Y.; Oh, T. S., Thermoelectric Power Generation Characteristics of a Thin-Film Device Consisting of Electrodeposited n-Bi2Te3 and p-Sb2Te3 Thin-Film Legs. *J. Electron. Mater.* **2013,** *42* (9), 2752-2757.